Non-Abelian Braiding of Dirac Fermionic Modes Using Topological Corner States in Higher-Order Topological Insulator

Yijia Wu,[1] Hua Jiang,[2,3] Jie Liu,[4] Haiwen Liu,[5] and X. C. Xie[1,6,7,*]

[1]International Center for Quantum Materials, School of Physics, Peking University, Beijing 100871, China
[2]School of Physical Science and Technology, Soochow University, Suzhou 215006, China
[3]Institute for Advanced Study, Soochow University, Suzhou 215006, China
[4]Department of Applied Physics, School of Science, Xian Jiaotong University, Xian 710049, China
[5]Center for Advanced Quantum Studies, Department of Physics, Beijing Normal University, Beijing 100875, China
[6]Beijing Academy of Quantum Information Sciences, Beijing 100193, China
[7]CAS Center for Excellence in Topological Quantum Computation, University of Chinese Academy of Sciences, Beijing 100190, China

(Received 9 January 2020; revised 13 April 2020; accepted 17 June 2020; published 13 July 2020)

We numerically demonstrate that the topological corner states residing in the corners of higher-order topological insulator possess non-Abelian braiding properties. Such topological corner states are Dirac fermionic modes other than Majorana zero modes. We claim that Dirac fermionic modes protected by nontrivial topology also support non-Abelian braiding. An analytical description on such non-Abelian braiding is conducted based on the vortex-induced Dirac-type fermionic modes. Finally, the braiding operators for Dirac fermionic modes, especially their explicit matrix forms, are analytically derived and compared with the case of Majorana zero modes.

DOI: 10.1103/PhysRevLett.125.036801

Introduction.—Higher-order topological insulator (HOTI) [1–4] has been drawing great attention for possessing novel boundary states including topological corner state [2,5,6] and topological hinge state [1,3]. As the bound state localized at the spatial boundary of the gapped 1D topological edge state, topological corner state can be viewed as an incarnation of the celebrated Jackiw-Rebbi zero mode [7–10] in 2D or 3D condensed matter systems. As one of the fascinating properties of Jackiw-Rebbi zero modes, the charge fractionalization has also been widely investigated for topological corner states in HOTI [1–3,6,11]. Another fascinating property of the Jackiw-Rebbi zero mode is its non-Abelian statistics [9,10,12,13] that a non-Abelian geometric phase highly related to the nontrivial topology is accumulated [14–16] during the braiding. The non-Abelian braiding statistics [17–19] is of great significance not only for its theoretical novelty beyond Fermi-Dirac statistics and Bose-Einstein statistics, but also for its possible application in the field of fault-tolerant topological quantum computation [19–24].

However, in the past three decades, the researches on the non-Abelian braiding statistics of quasiparticles in condensed matter systems mainly concentrated on the Majorana zero mode (MZM) [17–20,25–29]. In the field of topological corner states in HOTI, the non-Abelian braiding statistics has also only been investigated when superconducting pairing potential is presented [16,26,30], in which the topological corner states are self-conjugate and therefore are actually MZMs [10,18,19,25]. Nevertheless, the Majorana condition is not indispensable for the non-Abelian statistics [10,31,32]. Moreover, with the superconductivity-free condition, the experimental device is generally easier to fabricate and with a larger bulk gap. In fact, the Majorana condition is absent for a number of platforms supporting topological corner states such as the higher-dimensional Su-Schrieffer-Heeger (SSH) lattice [2,8,33] and the graphenelike structure [5,11]. In view of this, it is of significant importance to investigate the possible non-Abelian statistics of topological corner states in a HOTI without superconductivity.

In this Letter, we first perform a numerical simulation demonstrating the non-Abelian braiding properties of the HOTI's topological corner states based on a 2D SSH model. Because of the absence of the Majorana condition, such topological corner states are actually Dirac fermionic modes protected by the topology. Such localized Dirac fermionic modes in 2D topological system also appear as the vortex-bounded states in a quantum anomalous Hall insulator (QAHI), where the non-Abelian nature of the topologically protected Dirac fermionic modes is proved in an analytical way. Compared with the MZMs, the degeneracy of the Dirac fermionic modes could be removed by local perturbations. Though such degeneracy lifting induces a unitary transformation of the eigenstate basis where the braiding matrices live, the non-Abelian nature of the Dirac fermionic modes still remains. Finally, we demonstrate that the braiding operators for Dirac fermionic modes

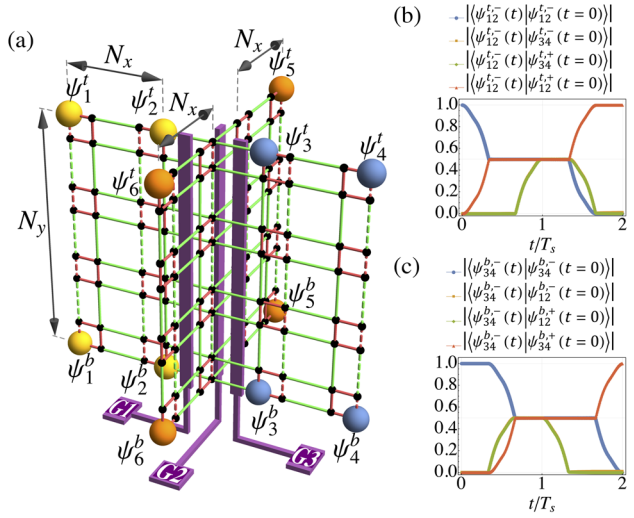

FIG. 1. (a) Sketch of the cross-shaped junction formed by four arms, each a 2D SSH square lattice in the size of $N_x \times N_y$ and three gates $G1$, $G2$, and $G3$. The red (green) bond denotes hopping strength γ (λ). The dashed bond denotes hopping term with negative sign. Spatial positions for the six pairs of topological corner states before braiding are shown as large spheres (three pairs on the top edge $\psi^t_{i=1,2,\ldots,6}$ and three pairs on the bottom edge $\psi^b_{i=1,2,\ldots,6}$, respectively). (b),(c) Evolution of the wave functions (b) $|\psi^{t,-}_{12}(t)\rangle$ and (c) $|\psi^{b,-}_{34}(t)\rangle$ during the whole braiding process that ψ^e_2 and ψ^e_3 ($e = t, b$) are swapped twice in succession. Parameters of the numerical calculations in (b) and (c) are $N_x = 5$, $N_y = 40$, $\lambda = 1.0$, $\gamma = 0.1$, and $T_s = 1200$.

as well as their matrix forms in the Fock space sectors are different from those of the MZMs [18] and the bosonic modes [32], although their geometric phases accumulated during the braiding have the same form.

Non-Abelian braiding of topological corner states.—As the minimal model of HOTI, the two-dimensional generalization [2,33] of the SSH model [8] is an ideal platform demonstrating the non-Abelian braiding properties of HOTI's topological corner states. The Hamiltonian of the 2D SSH model, $h_{\mathrm{SSH}}(\mathbf{p}) = (\gamma + \lambda\cos p_x)\tau_x\sigma_0 - \lambda\sin p_x\tau_y\sigma_z - (\gamma + \lambda\cos p_y)\tau_y\sigma_y - \lambda\sin p_y\tau_y\sigma_x$ [2], can be discretized in a square lattice (τ and σ for Pauli matrices), in which gapped 1D topological edge states and four topological corner states are presented in the nontrivial phase $|\gamma/\lambda| < 1$. Remarkably, each plaquette in this 2D SSH model contains a π flux.

A cross-shaped junction supporting the braiding operation [10,27,34] is composed of four arms, each a topologically nontrivial 2D SSH lattice with the size of $N_x \times N_y$, and three voltage gates ($G1$, $G2$, and $G3$) located near the cross point [Fig. 1(a)]. Each arm of this junction can be isolated from the others by the potential barrier induced by the presence of the corresponding gate voltage. For example, before the braiding, gate voltages in $G1$ and $G3$ are turned on, while gate voltage in $G2$ is turned off; therefore the cross-shaped junction is divided into three separated parts and 12 topological corner states ψ^e_i are presented as shown in Fig. 1(a) [edge index $e = t(b)$ for corner states on the top (bottom) edge, $i = 1, 2, \ldots, 6$]. Here we choose $N_y \gg N_x > \xi$, where ξ is the localization length of the topological corner states. In this way, the coupling between the top and the bottom edges can be neglected; hence, these 12 corner states are separated into two identical sets as ψ^t_i's on the top edge and ψ^b_j's on the bottom edge ($i, j = 1, 2, \ldots, 6$). By adiabatically [35] tuning the gate voltages in three steps [10,27,34], the spatial positions of two topological corner states ψ^t_2 and ψ^t_3 as well as the positions of ψ^b_2 and ψ^b_3 can be swapped simultaneously. In the first step, the gate voltage in $G1$ is adiabatically turned off at first, so that both ψ^t_2 and ψ^b_2 become extended states spatially distributed across two arms. After that, the gate voltage in $G2$ is adiabatically turned on; therefore ψ^t_2 (ψ^b_2) becomes localized on the top (bottom) edge at the back side of $G2$. In the second step, $G3$ is adiabatically turned off and then $G1$ is adiabatically turned on; hence ψ^t_3 (ψ^b_3) moves to the initial position of ψ^t_2 (ψ^b_2). In the final step, the swapping is accomplished by adiabatically turning off $G2$ then turning on $G3$ (for schematic illustration of the braiding process, see Supplemental Material [35]). The time cost for such swapping process is T_s.

Because of the finite-size-induced coupling between ψ^e_{2i-1} and ψ^e_{2i} ($e = t, b$, $i = 1, 2, 3$), the eigenstates of the cross-shaped junction before braiding ($t = 0$) are symmetric and antisymmetric states as $\psi^{e,\pm}_{12} = (1/\sqrt{2})(\psi^e_1 \pm e^{-i\alpha^e_{12}}\psi^e_2)$ and $\psi^{e,\pm}_{34} = (1/\sqrt{2})(\psi^e_4 \pm e^{-i\alpha^e_{34}}\psi^e_3)$, where α^e_{12} and α^e_{34} are arbitrary phases [12]. During the whole braiding process, ψ^e_2 and ψ^e_3 ($e = t, b$) are swapped twice in succession. Though all these corner states eventually come back to their initial spatial positions, the eigenstate before braiding $|\psi^{e,\pm}_{2i-1,2i}(t=0)\rangle$ evolves into $|\psi^{e,\pm}_{2i-1,2i}(t)\rangle = U(t)|\psi^{e,\pm}_{2i-1,2i}(t=0)\rangle$, where $U(t) = \hat{T}\exp[i\int_0^t d\tau H(\tau)]$ is the time evolution operator ($\hat{T}$ for time-ordering operator). For example, the eigenstate $|\psi^{t,-}_{12}(t=0)\rangle$ before braiding evolves into another eigenstate as $|\psi^{t,-}_{12}(t=2T_s)\rangle = |\psi^{t,+}_{12}(t=0)\rangle$ [Fig. 1(b)], implying that an additional π phase is picked up as $\psi^t_2 \to -\psi^t_2$. In the same way, by investigating the time evolution of other eigenstates [e.g., $|\psi^{b,-}_{34}(t)\rangle$ in Fig. 1(c)], we confirm that $\psi^e_2 \to -\psi^e_2$ and $\psi^e_3 \to -\psi^e_3$ after ψ^e_2 and ψ^e_3 are swapped twice in succession ($e = t, b$). As a result, if ψ^e_2 and ψ^e_3 are swapped once only, their non-Abelian nature is exhibited as $\psi^e_2 \to \psi^e_3$ and $\psi^e_3 \to -\psi^e_2$ (up to a gauge transformation). In brief, the topological corner states here are two identical sets of Dirac fermionic modes being braided simultaneously and exhibiting identical braiding properties.

Such braiding properties are reminiscent of the fact that swapping two MZMs γ_2 and γ_3 leads to $\gamma_2 \to \gamma_3$ and $\gamma_3 \to -\gamma_2$ [18]. However, a significant difference between MZMs and Dirac fermionic modes is that the zero-energy degeneracy between MZMs is protected by the

superconductivity-related particle-hole symmetry, while the degeneracy between Dirac fermionic modes could be lifted by local perturbations (if the local perturbations break the particle-hole-like symmetry of the 2D SSH lattice). For instance, in the presence of local perturbations, the effective Hamiltonian describing ψ_1^t and ψ_2^t is generally modified as

$$H_{\text{eff}} = (\mu+\Delta)(\psi_1^t)^\dagger\psi_1^t + (\mu-\Delta)(\psi_2^t)^\dagger\psi_2^t + [\epsilon_{12}e^{i\alpha_{12}^t}(\psi_1^t)^\dagger\psi_2^t + \text{H.c.}], \quad (1)$$

where $\mu \pm \Delta$ are the perturbation-induced on-site energies for ψ_1^t and ψ_2^t, respectively. The eigenstates formed by ψ_1^t and ψ_2^t are now in the new forms as $\varphi_{12}^{t,\pm} = (1/\sqrt{2})\{[\cos(\delta/2) \pm \sin(\delta/2)]\psi_1^t + e^{-i\alpha_{12}^t}[\pm\cos(\delta/2) - \sin(\delta/2)]\psi_2^t\}$ with eigenenergies $\epsilon_{12}^{\pm} = \mu \pm \sqrt{\Delta^2+\epsilon_{12}^2}$, where $\delta \in [-(\pi/2),(\pi/2)]$ is defined as $\sin\delta = (\Delta/\epsilon_{12})/\sqrt{(\Delta/\epsilon_{12})^2+1}$ and $\cos\delta = 1/\sqrt{(\Delta/\epsilon_{12})^2+1}$. Consequently, the degeneracy lift leads to a unitary transformation between the new set of eigenstates $\varphi_{12}^{t,\pm}$ and the former set of the eigenstates $\psi_{12}^{t,\pm}$:

$$\begin{pmatrix}\varphi_{12}^{t,-}\\ \varphi_{12}^{t,+}\end{pmatrix} = \begin{pmatrix}\cos\frac{\delta}{2} & -\sin\frac{\delta}{2}\\ \sin\frac{\delta}{2} & \cos\frac{\delta}{2}\end{pmatrix}\begin{pmatrix}\psi_{12}^{t,-}\\ \psi_{12}^{t,+}\end{pmatrix}. \quad (2)$$

However, the non-Abelian statistics describing the noncommutativity of the braiding operations does not depend on the specific choice of the set of eigenstates. In fact, numerical simulation has shown that swapping ψ_2^t and ψ_3^t twice in succession will lead to $|\varphi_{12}^{t,-}(t=2T_s)\rangle = -\sin\delta|\varphi_{12}^{t,-}(t=0)\rangle + \cos\delta|\varphi_{12}^{t,+}(t=0)\rangle$ in the presence of disorder effect [10]. It is still equivalent to the previously proved braiding properties $\psi_2^t \to \psi_3^t$ and $\psi_3^t \to -\psi_2^t$ when ψ_2^t and ψ_3^t are swapped once. From another point of view, the geometric phase accumulated during the braiding is independent of the degeneracy; the only thing we need to be concerned with is the nonvanishing dynamic phase due to the energy deviation (experimentally, it might be eliminated by symmetric braiding protocol [51]). Consequently, the non-Abelian nature remains valid even if the degeneracy is removed, though the experimental observables may change their forms.

Analytical description on the non-Abelian braiding.—Although the non-Abelian braiding properties of HOTI's topological corner states have been numerically demonstrated, an analytical description on such braiding, especially on the relation between the non-Abelian braiding and the nontrivial topology, is still highly needed. We note that the wave function of the topological corner state, for example, in the lower left-hand corner of the 2D SSH lattice and with vanishing momentum, has the form of $\psi^{\text{cor}}(x,y) = C^{\text{cor}}(e^{-x/\xi_+^{\text{cor}}} - e^{-x/\xi_-^{\text{cor}}})(e^{-y/\xi_+^{\text{cor}}} - e^{y/\xi_-^{\text{cor}}})(0,1,0,0)^T$, where $\xi_\pm^{\text{cor}} = [1 \pm \sqrt{1-2(1+\gamma/\lambda)}/2(1+\gamma/\lambda)]$ are the localization lengths ($\gamma/\lambda > -1$ is required) and C^{cor} is the normalization constant. The spatial part of such wave function is reminiscent of the other Dirac-type topological states, such as the vortex-induced bound state [31,52,53], which is also a zero-dimensional localized state in a 2D topological system. The Dirac-type bound state possessing zero energy is presented with the half-flux vortex, which is also in parallel with the π flux in each plaquette of the 2D SSH model. As we will show below, the 2D topological system with vortices could be served as an additional model proving the non-Abelian nature of the topologically protected Dirac fermionic modes in an analytical fashion. (In comparison, the swap of particles' spatial positions is prohibited in a strict 1D system.)

Specifically, considering a QAHI, $h_{\text{QAHI}}(\mathbf{p}) = A(p_x\sigma_x - p_y\sigma_y) + (M - B\mathbf{p}^2)\sigma_z$ [54,55], with two holes punched, where the first hole is placed at the origin, while the second one is at $\mathbf{q}$ [Fig. 2(a)]. Both holes have a radius R ($R \ll |\mathbf{q}|$) and are threaded by half-flux $\phi = \phi_0/2$ ($\phi_0 = h/e$ for flux quantum) so that two vortices are formed. A Dirac fermionic mode [53] with vanishing momentum is localized at the first vortex as $\psi_1^{\text{vor}}(\mathbf{r}) = (C^{\text{vor}}/\sqrt{r})[e^{-(r-R)/\xi_+^{\text{vor}}} - e^{-(r-R)/\xi_-^{\text{vor}}}]\exp[-(ie/\hbar)\Omega(\mathbf{r})](e^{i\theta}, i)^T$, where $\xi_\pm^{\text{vor}} = (A \pm \sqrt{A^2 - 4MB}/2M)$ are the localization lengths and C^{vor} is the normalization constant [35]. The vector potential induced by the second vortex has been taken into consideration as the gauge field [35,56],

$$\Omega(\mathbf{r}) = \begin{cases} \frac{\hbar}{2e}\arctan\left[\frac{(\mathbf{r}-\mathbf{q})\cdot\hat{y}}{(\mathbf{r}-\mathbf{q})\cdot\hat{x}}\right] & (\mathbf{r}-\mathbf{q})\cdot\hat{x} > 0 \\ \frac{\hbar}{2e}\left\{\arctan\left[\frac{(\mathbf{r}-\mathbf{q})\cdot\hat{y}}{(\mathbf{r}-\mathbf{q})\cdot\hat{x}}\right] + \pi\right\} & (\mathbf{r}-\mathbf{q})\cdot\hat{x} < 0, \end{cases} \quad (3)$$

where $\hat{x}$, $\hat{y}$ denotes the unit vector along the x and y direction, respectively. There is a branch cut [18] of the gauge field $\Omega(\mathbf{r})$ along the $-\hat{y}$ direction [Fig. 2(b)] and the phase jump across the branch cut is $\pi\hbar/e$.

Similarly, the wave function of the Dirac fermionic mode bounded with the second vortex is denoted as $\psi_2^{\text{vor}}(\mathbf{r}-\mathbf{q})$, in which the gauge field induced by the first vortex has also been included. If the (relative) spatial positions of these two vortices are swapped through a counterclockwise rotation,

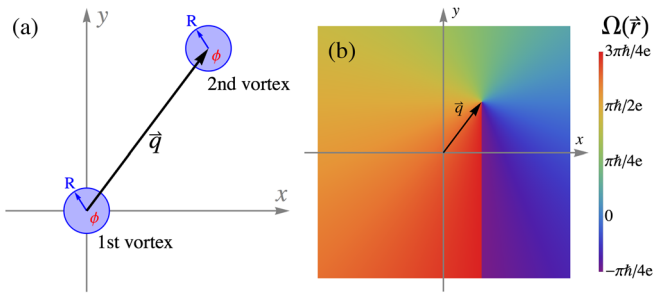

FIG. 2. (a) Schematic plot of two vortices with radius R and magnetic flux $\phi = \phi_0/2 = \pi\hbar/e$ threaded in a QAHI. (b) Gauge field $\Omega(\mathbf{r})$ with a branch cut along the $-\hat{y}$ direction.

then the first Dirac fermionic mode passes through the branch cut of the second vortex [18] and acquires an additional π phase, while the second Dirac fermionic mode does not go through the branch cut of the first vortex (see Supplemental Material [35] for schematic plot). Therefore, we analytically obtain the braiding properties of these Dirac fermionic modes as

$$\psi_1^{\mathrm{vor}}(\mathbf{r}) \to \psi_2^{\mathrm{vor}}(\mathbf{r}-\mathbf{q}), \psi_2^{\mathrm{vor}}(\mathbf{r}-\mathbf{q}) \to -\psi_1^{\mathrm{vor}}(\mathbf{r}), \quad (4)$$

which is exactly the same as the topological corner states in HOTI as expected. This analytical derivation unambiguously demonstrates that the non-Abelian braiding here comes from the flux-induced geometric phase. We conclude that non-Abelian braiding can also be exhibited for Dirac fermionic modes, provided that nontrivial topology [14,15] is presented. Remarkably, identical non-Abelian behaviors are also presented for half-flux vortices in quantum spin Hall insulator (2D TI) [52], which is two copies of QAHIs related by time-reversal (TR) symmetry.

Braiding operator for Dirac fermionic mode.—Based on the investigation on both the topological corner states in HOTI and the Dirac-type bound states in QAHI, we have shown that an operation T_i swapping two Dirac fermionic modes ψ_i and ψ_{i+1} will give rise to $\psi_i \to \psi_{i+1}$, $\psi_{i+1} \to -\psi_i$, $\psi_j \to \psi_j$ ($j \neq i$ and $j \neq i+1$), which is similar to the braiding properties of MZM [18] and bosonic mode [32]. Nevertheless, the braiding operator $\tau(T_i)$ for Dirac fermionic modes obeying $\tau(T_i)\psi_j[\tau(T_i)]^{-1} = T_i(\psi_j)$ has the explicit form of

$$\tau(T_i) = \exp\left[\frac{\pi}{2}(\psi_{i+1}^\dagger \psi_i - \psi_i^\dagger \psi_{i+1})\right], \quad (5)$$

in which $\tau(T_i)\psi_i[\tau(T_i)]^{-1} = \psi_{i+1}$ as well as $\tau(T_i)\psi_{i+1}[\tau(T_i)]^{-1} = -\psi_i$ can be proved by adopting the Baker-Hausdorff formula [35]. In comparison, the braiding operators are $\tau(T_i) = \exp[(\pi/2)(b_{i+1}^\dagger b_i - b_i^\dagger b_{i+1})]$ for bosonic mode [32] and $\tau(T_i) = \exp[(\pi/4)\gamma_{i+1}\gamma_i]$ for MZM [18], where b_i and γ_i are bosonic and Majorana operators, respectively. If each Dirac fermionic mode is decomposed into two MZMs with different "flavors" as $\psi_i \equiv \frac{1}{2}(\gamma_i^a + i\gamma_i^b)$ (a, b for flavor indices), then the equivalent form of Eq. (5) as $\tau(T_i) = \exp[(\pi/4)\gamma_{i+1}^a\gamma_i^a]$ $\exp[(\pi/4)\gamma_{i+1}^b\gamma_i^b]$ is the tensor product of Majorana braiding operator with different flavors.

Such tensor product form implies that the crucial difference between the non-Abelian statistics of the MZM and the Dirac fermionic mode lies in their quantum dimensions. For instance, for a Majorana system composed of four MZMs, the quantum dimension is $2^2 = 4$ and its Fock space could be divided into two two-dimensional sectors with different fermion parities. All the braiding operators are block diagonal because the braiding operations conserve the fermion parity [18]. Moreover, the braiding operators have very similar matrix forms in both these two sectors [18]. In contrast, the Fock space for a fermionic system composed of four Dirac fermionic modes (ψ_1, ψ_2, ψ_3, and ψ_4) is in the quantum dimension of $2^4 = 16$ [31]. Such a Fock space can be divided into five sectors, each labeled by a different fermion number $N_f = 0, 1, 2, 3, 4$ and with a different quantum dimension $C_4^0, C_4^1, C_4^2, C_4^3, C_4^4$. The Dirac fermionic modes exhibit distinctly different braiding properties in each of these sectors. As an extreme example, the sector with fermion number $N_f = 4$ is one dimensional as $\psi_1^\dagger\psi_2^\dagger\psi_3^\dagger\psi_4^\dagger|0\rangle$; therefore all the braiding operations will only give rise to a trivial factor so that the non-Abelian braiding statistics is absent.

In contrast, the non-Abelian braiding properties are well exhibited in other sectors with $N_f = 1$, 2, or 3. For illustration, in the single-fermion sector, considering that these four fermionic modes are coupled in the manner of $\psi_{12}^\pm = (1/\sqrt{2})(\psi_1 \pm e^{-i\alpha_{12}}\psi_2)$ and $\psi_{34}^\pm = (1/\sqrt{2})$ $(\psi_4 \pm e^{-i\alpha_{34}}\psi_3)$, the four-dimensional single-fermion sector can be spanned as $[(\psi_{12}^-)^\dagger|0\rangle, (\psi_{12}^+)^\dagger|0\rangle, (\psi_{34}^-)^\dagger|0\rangle,$ $(\psi_{34}^+)^\dagger|0\rangle]^T$. Without loss of generality, here we set $\alpha_{12} = \alpha_{34} = (\pi/2)$ (see Supplemental Material [35] for general discussions), so that Eq. (5) gives rise to $\tau(T_1) = \exp[(i\pi/2)(\psi_{12}^-)^\dagger\psi_{12}^- - (i\pi/2)(\psi_{12}^+)^\dagger\psi_{12}^+]$; hence $\tau(T_1)(\psi_{12}^\pm)^\dagger|0\rangle = \mp i(\psi_{12}^\pm)^\dagger|0\rangle$ as well as $\tau(T_1)(\psi_{34}^\pm)^\dagger|0\rangle = (\psi_{34}^\pm)^\dagger|0\rangle$ can be obtained. In such way, we could write down the matrix forms of the braiding operators in the single-fermion basis $[(\psi_{12}^-)^\dagger|0\rangle, (\psi_{12}^+)^\dagger|0\rangle, (\psi_{34}^-)^\dagger|0\rangle,$ $(\psi_{34}^+)^\dagger|0\rangle]^T$ as

$$\tau(T_1) = \begin{pmatrix} i\sigma_z & 0 \\ 0 & \sigma_0 \end{pmatrix}, \qquad \tau(T_3) = \begin{pmatrix} \sigma_0 & 0 \\ 0 & i\sigma_z \end{pmatrix}$$

(σ for Pauli matrix), and

$$\tau(T_2) = \frac{1}{2}\begin{pmatrix} 1 & 1 & 1 & -1 \\ 1 & 1 & -1 & 1 \\ -1 & 1 & 1 & 1 \\ 1 & -1 & 1 & 1 \end{pmatrix}, \quad (6)$$

respectively. All of the two-qubit Pauli rotations [21] $\sigma_i \otimes \sigma_j$ ($i, j = 0, 1, 2, 3$) can be implemented (up to an overall phase) by combining swapping operations T_1, T_2, and T_3. Such two-qubit Pauli rotations are naturally the combination of the single-qubit operations on each set of MZMs with different flavors. It is worth noting that the $\tau(T_2)$ in Eq. (6) is consistent with the numerical results on the braiding of HOTI's topological corner states [Figs. 1(b) and 1(c)] that $|\psi_{12}^{t,-}(t = T_s)\rangle$ is the equally weighted superposition of both $|\psi_{12}^{t,\pm}(t = 0)\rangle$ and $|\psi_{34}^{t,\pm}(t = 0)\rangle$ when ψ_2^e and ψ_3^e ($e = t$, b) are swapped once ($t = T_s$). More importantly, $\tau(T_2)$ commutes with neither $\tau(T_1)$ nor $\tau(T_3)$, indicating that they cannot be diagonalized simultaneously by any unitary transformation. Such a nondiagonal

braiding matrix mathematically displays the non-Abelian nature of the Dirac fermionic modes in an unambiguous way. Finally, in the double-fermion ($N_f = 2$) or triple-fermion sector ($N_f = 3$), the non-Abelian nature of the braiding operators could also be proved in a similar way [35].

Discussion.—We have demonstrated the non-Abelian braiding properties of topological corner states, a kind of Dirac fermionic mode protected by nontrivial topology in HOTI. The non-Abelian nature of the topologically protected Dirac fermionic mode is proved to be highly related to its nontrivial topology. The braiding operators of the Dirac fermionic modes have also been explicitly expressed. Additionally, these braiding operators are in the distinctly different matrix forms in the basis with different fermion number. This is in stark contrast to the MZMs whose braiding operators are in the similar matrix forms in the basis of different fermion parity. Alternatively, the Dirac fermionic modes in our Letter could be viewed as a composite [56] composed of electron and vortex. In this way, we can argue that these Dirac fermionic states are effectively many-body states consisting of both electrons and vortices as quasiparticles.

Experimentally, the 2D SSH lattice as well as the braiding operations may be realized through a cross-shaped junction constructed by topological electric circuit [57–60]. The detailed experimental scheme is exhibited in the Supplemental Material [35].

We thank Chui-Zhen Chen, Jin-Hua Gao, Qing-Feng Sun, and Zhi-Qiang Zhang for fruitful discussion. This work is financially supported by the National Basic Research Program of China (Grants No. 2015CB921102, No. 2017YFA0303301, No. 2019YFA0308403, and No. 2017YFA0304600), the National Natural Science Foundation of China (Grants No. 11534001, No. 11674028, No. 11822407, and No. 11974271), and the Strategic Priority Research Program of Chinese Academy of Sciences (Grant No. XDB28000000).

*Corresponding author.
xcxie@pku.edu.cn

[1] F. Schindler, A. M. Cook, M. G. Vergniory, Z. Wang, S. S. Parkin, B. A. Bernevig, and T. Neupert, Sci. Adv. **4**, eaat0346 (2018).
[2] W. A. Benalcazar, B. A. Bernevig, and T. L. Hughes, Science **357**, 61 (2017).
[3] G. van Miert and C. Ortix, Phys. Rev. B **98**, 081110(R) (2018).
[4] L. Trifunovic and P. W. Brouwer, Phys. Rev. X **9**, 011012 (2019).
[5] Y. Yang, Z. Jia, Y. Wu, Z.-H. Hang, H. Jiang, and X. C. Xie, Sci. Bull. **65**, 531 (2020).
[6] W. A. Benalcazar, T. Li, and T. L. Hughes, Phys. Rev. B **99**, 245151 (2019).
[7] R. Jackiw and C. Rebbi, Phys. Rev. D **13**, 3398 (1976).
[8] W. P. Su, J. R. Schrieffer, and A. J. Heeger, Phys. Rev. Lett. **42**, 1698 (1979).
[9] J. Klinovaja and D. Loss, Phys. Rev. B **92**, 121410(R) (2015).
[10] Y. Wu, H. Liu, J. Liu, H. Jiang, and X. C. Xie, Natl. Sci. Rev. **7**, 572 (2019).
[11] C.-Y. Hou, C. Chamon, and C. Mudry, Phys. Rev. Lett. **98**, 186809 (2007).
[12] J. Klinovaja and D. Loss, Phys. Rev. Lett. **110**, 126402 (2013).
[13] P. Boross, J. K. Asbóth, G. Széchenyi, L. Oroszlány, and A. Pályi, Phys. Rev. B **100**, 045414 (2019).
[14] F. von Oppen, Y. Peng, and F. Pientka, Topological superconducting phases in one dimension, in *Topological Aspects of Condensed Matter Physics*, Lecture Notes of the Les Houches Summer School, 2014 Vol. 103 (Oxford University Press, Oxford,2017), p. 387.
[15] V. Lahtinen and J. K. Pachos, SciPost Phys. **3**, 021 (2017).
[16] M. Ezawa, Phys. Rev. B **100**, 045407 (2019).
[17] G. Moore and N. Read, Nucl. Phys. **B360**, 362 (1991).
[18] D. A. Ivanov, Phys. Rev. Lett. **86**, 268 (2001).
[19] J. Alicea, Y. Oreg, G. Refael, F. Von Oppen, and M. P. Fisher, Nat. Phys. **7**, 412 (2011).
[20] C. Nayak, S. H. Simon, A. Stern, M. Freedman, and S. Das Sarma, Rev. Mod. Phys. **80**, 1083 (2008).
[21] J. K. Pachos, *Introduction to Topological Quantum Computation* (Cambridge University Press, Cambridge, England, 2012).
[22] B. Lian, X.-Q. Sun, A. Vaezi, X.-L. Qi, and S.-C. Zhang, Proc. Natl. Acad. Sci. U.S.A. **115**, 10938 (2018).
[23] A. Y. Kitaev, Ann. Phys. (Amsterdam) **303**, 2 (2003).
[24] S. Das Sarma, M. Freedman, and C. Nayak, Phys. Rev. Lett. **94**, 166802 (2005).
[25] A. Y. Kitaev, Phys. Usp. **44**, 131 (2001).
[26] T. E. Pahomi, M. Sigrist, and A. A. Soluyanov, arXiv:1904.07822.
[27] C. S. Amorim, K. Ebihara, A. Yamakage, Y. Tanaka, and M. Sato, Phys. Rev. B **91**, 174305 (2015).
[28] R. Willett, J. P. Eisenstein, H. L. Störmer, D. C. Tsui, A. C. Gossard, and J. H. English, Phys. Rev. Lett. **59**, 1776 (1987).
[29] W. Pan, J.-S. Xia, V. Shvarts, D. E. Adams, H. L. Stormer, D. C. Tsui, L. N. Pfeiffer, K. W. Baldwin, and K. W. West, Phys. Rev. Lett. **83**, 3530 (1999).
[30] M. Ezawa, arXiv:1907.06911.
[31] S. Yasui, K. Itakura, and M. Nitta, Nucl. Phys. **B859**, 261 (2012).
[32] T. Iadecola, T. Schuster, and C. Chamon, Phys. Rev. Lett. **117**, 073901 (2016).
[33] F. Liu and K. Wakabayashi, Phys. Rev. Lett. **118**, 076803 (2017).
[34] C.-Z. Chen, Y.-M. Xie, J. Liu, P. A. Lee, and K. T. Law, Phys. Rev. B **97**, 104504 (2018).
[35] See Supplemental Material at http://link.aps.org/supplemental/10.1103/PhysRevLett.125.036801 for technical details about the numerical simulation on non-Abelian braiding, derivation of the vortex-bounded Dirac fermionic modes' wave function, braiding operator and braiding matrix, and the realization of non-Abelian braiding in topological circuit, which includes Refs. [36–50].

[36] J. D. Sau, D. J. Clarke, and S. Tewari, Phys. Rev. B **84**, 094505 (2011).
[37] V. V. Albert, L. I. Glazman, and L. Jiang, Phys. Rev. Lett. **114**, 173902 (2015).
[38] C. H. Lee, S. Imhof, C. Berger, F. Bayer, J. Brehm, L. W. Molenkamp, T. Kiessling, and R. Thomale, Commun. Phys. **1**, 39 (2018).
[39] Z.-Q. Zhang, B.-L. Wu, J. Song, and H. Jiang, Phys. Rev. B **100**, 184202 (2019).
[40] K. Luo, R. Yu, H. Weng *et al.*, Research **2018**, 6793752 (2018).
[41] E. Zhao, Ann. Phys. (Amsterdam) **399**, 289 (2018).
[42] R. Yu, Y. Zhao, and A. P. Schnyder,Natl. Sci. Rev. (2020) https://doi.org/10.1093/nsr/nwaa065.
[43] F. Schindler, Z. Wang, M. G. Vergniory, A. M. Cook, A. Murani, S. Sengupta, A. Y. Kasumov, R. Deblock, S. Jeon, I. Drozdov *et al.*, Nat. Phys. **14**, 918 (2018).
[44] M. Serra-Garcia, V. Peri, R. Süsstrunk, O. R. Bilal, T. Larsen, L. G. Villanueva, and S. D. Huber, Nature (London) **555**, 342 (2018).
[45] X. Zhang, H.-X. Wang, Z.-K. Lin, Y. Tian, B. Xie, M.-H. Lu, Y.-F. Chen, and J.-H. Jiang, Nat. Phys. **15**, 582 (2019).
[46] X. Ni, M. Weiner, A. Alù, and A. B. Khanikaev, Nat. Mater. **18**, 113 (2019).
[47] H. Xue, Y. Yang, F. Gao, Y. Chong, and B. Zhang, Nat. Mater. **18**, 108 (2019).
[48] C. W. Peterson, W. A. Benalcazar, T. L. Hughes, and G. Bahl, Nature (London) **555**, 346 (2018).
[49] B.-Y. Xie, G.-X. Su, H.-F. Wang, H. Su, X.-P. Shen, P. Zhan, M.-H. Lu, Z.-L. Wang, and Y.-F. Chen, Phys. Rev. Lett. **122**, 233903 (2019).
[50] X.-D. Chen, W.-M. Deng, F.-L. Shi, F.-L. Zhao, M. Chen, and J.-W. Dong, Phys. Rev. Lett. **122**, 233902 (2019).
[51] T. Yan, B.-J. Liu, K. Xu, C. Song, S. Liu, Z. Zhang, H. Deng, Z. Yan, H. Rong, K. Huang *et al.*, Phys. Rev. Lett. **122**, 080501 (2019).
[52] W.-Y. Shan, J. Lu, H.-Z. Lu, and S.-Q. Shen, Phys. Rev. B **84**, 035307 (2011).
[53] S.-Q. Shen, *Topological Insulators* (Springer, Berlin, 2012).
[54] B. A. Bernevig, T. L. Hughes, and S.-C. Zhang, Science **314**, 1757 (2006).
[55] X.-L. Qi and S.-C. Zhang, Rev. Mod. Phys. **83**, 1057 (2011).
[56] F. Wilczek, Phys. Rev. Lett. **49**, 957 (1982).
[57] S. Imhof, C. Berger, F. Bayer, J. Brehm, L. W. Molenkamp, T. Kiessling, F. Schindler, C. H. Lee, M. Greiter, T. Neupert *et al.*, Nat. Phys. **14**, 925 (2018).
[58] M. Serra-Garcia, R. Süsstrunk, and S. D. Huber, Phys. Rev. B **99**, 020304(R) (2019).
[59] M. Ezawa, Phys. Rev. B **98**, 201402(R) (2018).
[60] J. Bao, D. Zou, W. Zhang, W. He, H. Sun, and X. Zhang, Phys. Rev. B **100**, 201406(R) (2019).